THERMODYNAMIC MODELING OF AN EPITROCHOIDAL ENGINE CYCLE

by

Thomas Allen Grammer, Jr

Submitted in partial fulfillment of the requirements for Departmental Honors in the Department of Engineering
Texas Christian University
Fort Worth, Texas

December 10, 2012

THERMODYNAMIC MODELING OF AN EPITROCHOIDAL ENGINE CYCLE

Project Approved:

Robert Bittle, Ph.D.
Department of Engineering
(Supervising Professor)

Steven Weis, Ph.D.
Department of Engineering

Loren Spice, Ph.D.
Department of Mathematics

TABLE OF CONTENTS

LIST OF FIGURES

DEFINITION OF VARIABLES

$\theta = Instantaneous\ Crankshaft\ angle\ from\ Top\ Dead\ Center\ (TDC)$

$\alpha = Instantaneous\ epitrochoidal\ offset\ angle\ from\ TDC$

$e = Crankshaft\ (CS)\ radius\ to\ ℄\ of\ crankpin$

$E = Epitrochoidal\ offset\ from\ crankpin\ to\ piston\ rod$

$R = Piston\ rod\ length$

$\sum = Instantaneous\ radius\ from\ CS\ to\ ℄\ of\ piston\ rod$

$\beta = Instantaneous\ angle\ from\ TDC\ to\ ℄\ of\ piston\ rod$

$X_\theta = Instantaneous\ dist.\ from\ CS\ ℄\ to\ top\ of\ piston\ rod$

$V_{min} = Cylinder\ Volume\ at\ Top\ Dead\ Center$

$V_{max} = Cylinder\ Volume\ at\ Bottom\ Dead\ Center$

$B = Cylinder\ Bore\ Diameter$

$P = Air\ Pressure$

$T = Air\ Temperature$

$S = Piston\ Stroke\ Length$

$h = Heat\ Transfer\ Coefficient$

$Area_s = Effective\ Cylinder\ Surface\ Area$

$A_{piston} = Surface\ Area\ of\ Piston\ Head$

$A_{head} = Affective\ Surface\ Area\ of\ Cylinder\ Head$

$T_{wall} = Cylinder\ Wall\ Temperature$

$\dot{Q}_{H/T_n} = Heat\ Transfer\ Rate$

$Q_{H/T_n} = Total\ Heat\ Transferred$

$Q_{C_n} = Total\ Heat\ of\ Combustion$

$u_n = Internal\ Energy$

$LHV = Lower\ Heating\ Value$

$W_{net} = Net\ Work$

ACKNOWLEDGEMENTS

I would like to thank the 2011 Texas Christian University Engineering Senior Design Project, (Julian Heinrich, et al.) for the tireless work and dedication which made this research successful. I am honored to have been part of the team.

INTRODUCTION

The Otto cycle, developed in the mid nineteenth century, modeled the maximum power output of a piston-cylinder spark ignition engine in an ideal case. Several limitations have been shown in practical application, however, that have further restricted the performance of small, naturally aspirated engines. These limitations have been the topic of much research over the past several decades.

One such non-ideal limitation, which lowered the useful power output of naturally aspirated engines, was the restriction caused by the open intake valve on the intake stroke. This restriction limits the airflow into the cylinder and results in a cylinder pressure less than atmospheric. To counter this difficulty and help engine performance at higher rotational speeds, the intake valve has often been allowed to remain open slightly longer, and close only once the piston had begun rising during the compression stroke. This delayed closing results in a trapped volume or "effective displacement" that is less than the ideal full cylinder displacement. The net result has been less fuel and air mass contained in the full cylinder volume than would be predicted by the Otto cycle, leading to a volumetric efficiency less than ideal.

The exhaust valve movement also reduces the power produced by an engine. To ensure the exhaust valve is fully or substantially open when the piston begins to rise in the exhaust stroke and avoid energy loss through compression of exhaust gasses, the exhaust valve often begins opening before the completion of the power stroke. This loss of cylinder pressure before the end of the power stroke reduces the amount of work produced by the high temperature expanding gasses.

In order to address these limitations found in a standard 4 stroke engine, the epitrochoidal engine design (developed and patented by Mark Venitozzi and Marozzi, LLC) utilizes a system of gears to change the path of the piston. Instead of a standard piston movement which is a symmetric sine function with respect to time, the epitrochoidal engine's piston moves in a path described by the sum of two sine waves. This eccentric path reaches top and bottom dead centers at the same time in the cycle as the standard path, but dwells at the bottom of the cylinder for a greater length of time before beginning its ascent (See Figure 1).

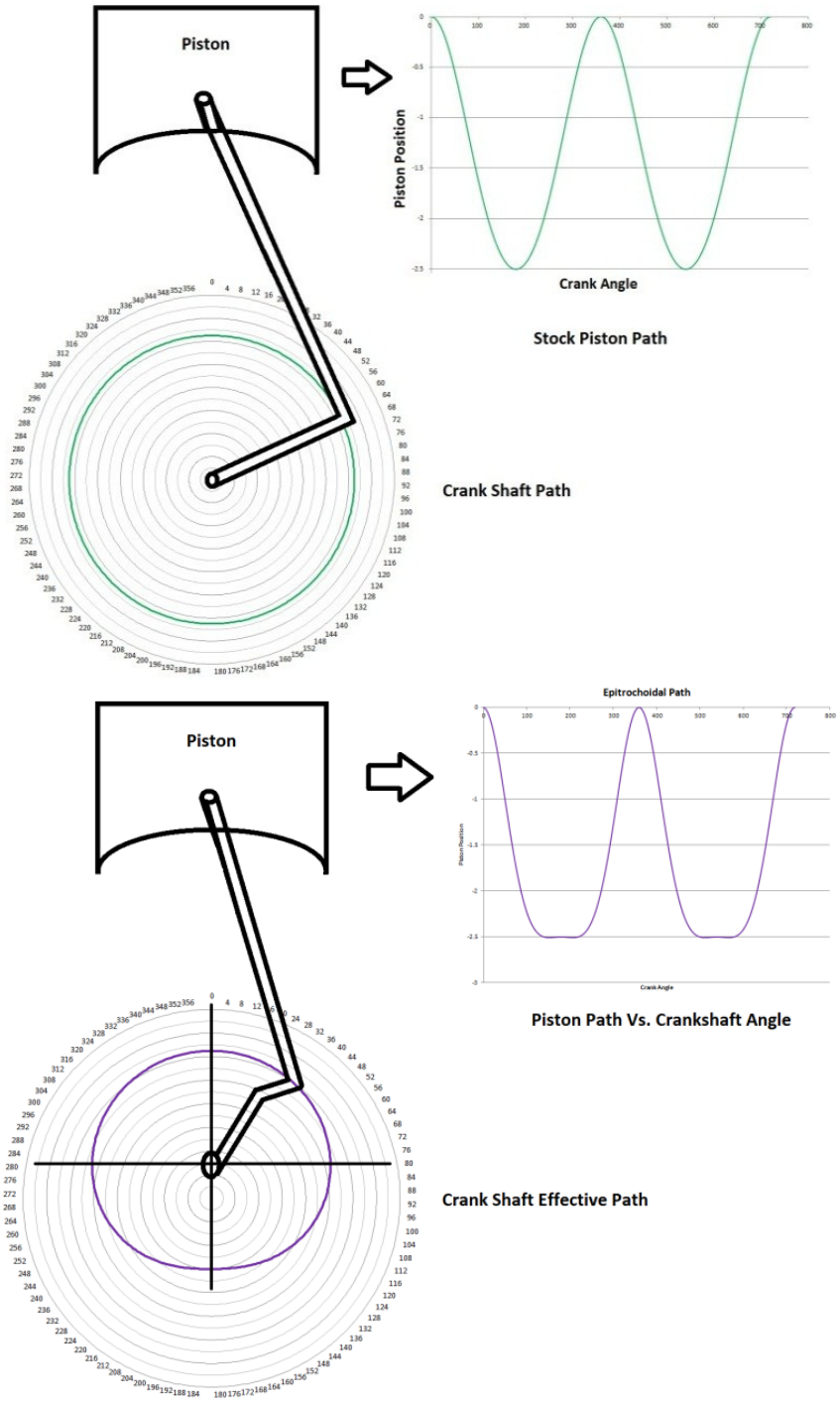

Figure 1. Comparison of crankshaft and piston path.

In addition, the rate of change in the volume during compression/exhaust and power/intake is greater. To reiterate, the pistons move faster in the stroke, but still arrive at TDC and BDC at the same time in the cycle as the standard path.

While the gearing required to create this path will induce additional friction losses, the proposed benefits of this change in piston path were predicted to increase the total power output of the engine over a standard path in several ways. First, because the piston dwells at the bottom of the stroke time is allowed for the intake valve to fully close before the piston began to rise during compression. This change increases the engine's effective displacement and volumetric efficiency. Second, as the piston falls faster and dwells at the bottom of the stroke during the intake stroke, a larger pressure difference is created between the air intake port and the inside of the cylinder. The larger pressure difference for a longer time enables the epitrochoidal engine cycle to achieve a higher volumetric efficiency in comparison to the standard cycle. Third, more work can be achieved during the power stroke. While the exhaust valve opens near the end of the power stroke at the same crank shaft angle for both engine designs, the piston travels farther during the same time when using the epitrochoidal cycle. This means that more work can be extracted from the high pressure gasses before the exhaust valve opens (See Figure 2).

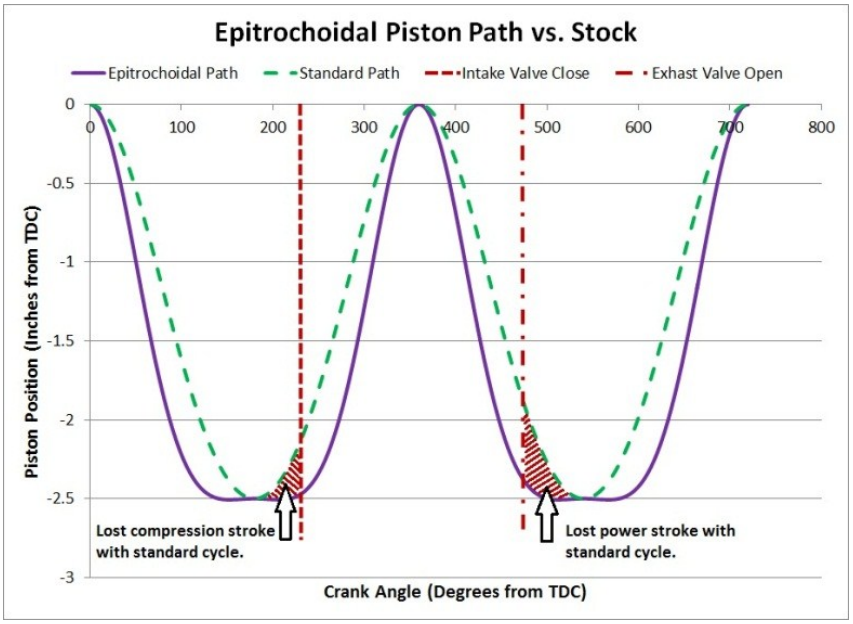

Figure 2. Piston path comparison with intake and exhaust movement added.

The increase in dwell time at the bottom of the epitrochoidal path was accomplished using an eccentric bearing between the crankshaft and the piston rod, which had been geared to rotate in the same direction as the crankshaft, but at twice the crankshaft rotational speed (See Figure 3).

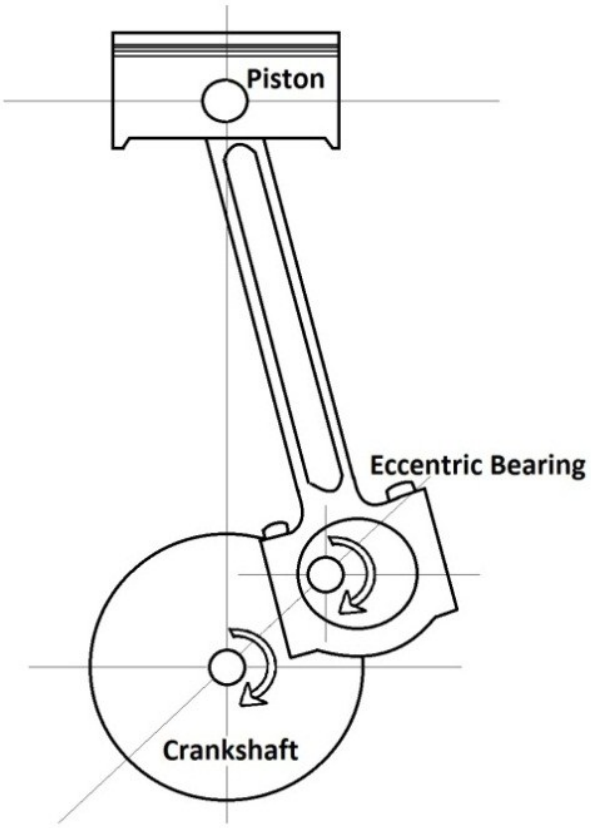

Figure 3. Basic Epitrochoidal Crankshaft Diagram

Within the comparative models, the change in the path was evaluated incrementally as the models were developed to see the effect of the path difference on the pressure volume diagram and the power output of the engine. These two discrete comparative models were used to evaluate the claimed performance benefit of the new epitrochoidal cycle using simple thermodynamic principles. In addition to theoretical thermodynamic calculations, empirical data for frictional losses was used to supplement the model and increase the accuracy of the output power predictions.

MATHEMATICAL MODEL OF PISTON PATH

To begin the thermodynamic analysis, characteristic equations of the standard and epitrochoidal motions were first derived. These characteristic equations (Equations 1 & 8) were developed using only basic, physical measurements and geometric constraints provided by a one-cylinder epitrochoidal prototype engine, and a standard cycle engine of the same displacement. (This equation was used in creating Figure 1.)

The standard cycle path originated from a simple diagram in two-dimensions, where the critical geometry of each component was retained, but the pinned joints in the system were allowed to change as the crankshaft angle varied (See Figure 4).

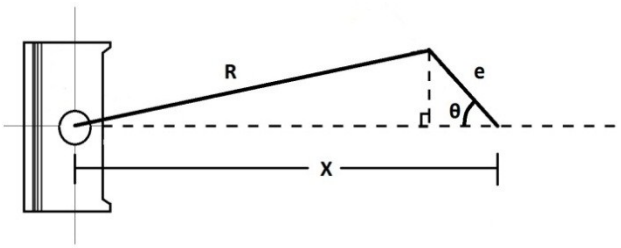

Figure 4. Standard Cycle Free Body Diagram

The distance to the top of the piston rod from the center of rotation of the crankshaft was assigned the distance 'X', which was simply the sum of the legs of two right triangles. These two right triangles are shown in Figure 4 and the resulting equation given in Equation 1.

$$X_\theta = e * \cos\theta + \sqrt{R^2 - [e * \sin\theta]^2} \quad (1)$$

This mathematical expression gave the movement of the piston with crankshaft angle in terms of the crankshaft radius, angle, and the piston rod length. This equation remained valid through a full 360° crankshaft rotation. The epitrochoidal path equation was calculated starting with an additional geometric element, the eccentric bearing. This bearing, rotating at twice the crankshaft rotational speed, was added to the standard cycle free body diagram (FBD) and the path equation derivation began. The FBD has been included in Figure 5.

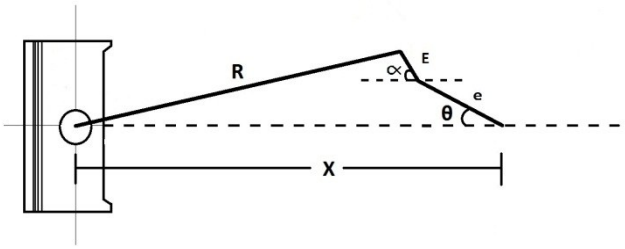

Figure 5. Epitrochoidal Cycle Free Body Diagram

The relationship between the changes in eccentric bearing angle α and crankshaft angle θ with time was given to be simply

$$\dot{\alpha} = 2\dot{\theta} \quad (2)$$

This linear rate dependence indicated that for any angle θ, the angle α was 2θ, where both α and θ begin at 0º.

In order to describe the piston position with crankshaft angle for the epitrochoidal cycle, the crankshaft and eccentric bearing linkages were combined. This combination recreated the model shown in Figure 4, but with the combined or 'sum' linkage then allowed to vary in length and angle from the original crankshaft linkage (See Figure 5). A detailed drawing of this sum (∑) linkage is shown in Figure 6.

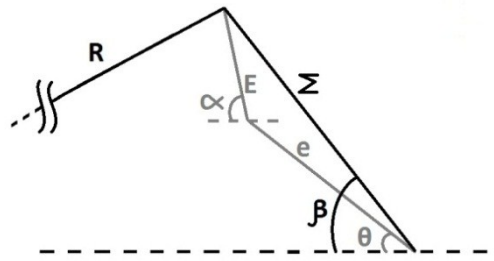

Figure 6. Epitrochoidal Sum Linkage Detail

The length of the sum linkage Σ was found by taking the horizontal and vertical components of both the crankshaft and eccentric bearing linkages and adding them together, respectively. Using the summed vertical and horizontal lengths to form a right triangle which had Σ as the hypotenuse, the Pythagorean Theorem could then be applied.

$$\sum = \sqrt{[e * \cos\theta + E * \cos\alpha]^2 + [e * \sin\theta + E * \sin\alpha]^2} \qquad (3)$$

Substituting $2 * \theta$ for α and simplifying yielded:

$$\sum = E * \sqrt{\left(\frac{e}{E}\right)^2 + 2 * \frac{e}{E} * \cos\theta + 1} \tag{4}$$

The angle β was found using the same vertical and horizontal components of both the crankshaft and eccentric bearing. The angle became simply the inverse tangent of the vertical component divided by the horizontal.

$$\beta = \tan^{-1}\left(\frac{e*\sin\theta + E*\sin\alpha}{e*\cos\theta + E*\cos\alpha}\right) \tag{5}$$

Substituting 2θ for α and simplifying yielded:

$$\beta = \tan^{-1}\left(\frac{e*\sin\theta + E*\sin 2\theta}{e*\cos\theta + E*\cos 2\theta}\right) \tag{6}$$

So, the piston position versus crankshaft angle for the epitrochoidal path in terms of ∑ and β was:

$$X_\theta = \sum * \cos\beta + \sqrt{R^2 - [\sum * \sin\beta]^2} \tag{7}$$

The piston position of the epitrochoidal engine could then be written solely as a function of measured physical parameters and crankshaft angle, θ. After substituting equation 4 for Σ, and equation 5 for β, and simplifying, the relation finally became the final epitrochoidal path equation:

$$X_\theta = e * \cos\theta + E * \cos 2\theta + \sqrt{R^2 - E^2 * \left(\sin\theta * \left[\frac{e}{E} + 2\cos\theta\right]\right)^2} \tag{8}$$

To calculate the cylinder volume in terms of piston position, the common minimum volume (at top dead center) was measured in the test engines, and the change in volume ΔV caused by crankshaft rotation was added.

$$V = V_{Min} + \Delta V \tag{9}$$

The change in volume with crankshaft angle was found to be simply the piston position at top dead center minus the piston position at the current crankshaft angle, with that difference multiplied by the cross-sectional area of the cylinder to obtain a volume.

$$\Delta V = (X_{TDC} - X_{\theta}) * \frac{\pi}{4} * B^2 \tag{10}$$

Substituting Equation 8 for X_{TDC} (where θ=0°) and X_{θ}, and simplifying, the volume was found as a function of crankshaft angle for the epitrochoidal cycle.

$$V = V_{Min} + \left\{R + e * (1 - \cos\theta) + E * (1 - \cos 2\theta) - \sqrt{R^2 - E^2 * \left(\sin\theta * \left[\frac{e}{E} + 2\cos\theta\right]\right)^2}\right\} * \frac{\pi}{4} * B^2 \tag{11}$$

COMPARATIVE THERMODYNAMIC MODEL

With the piston position and volume versus crankshaft angle described mathematically, a simple, discrete thermodynamic Otto cycle was created for both the standard and epitrochoidal crank pin paths. For the development of the models, an engine speed of 3600 RPM was chosen, and a stoichiometric mixture of fuel and air was assumed to be supplied from the carburetor at atmospheric pressure.

Using Microsoft Excel®, two cycle paths were created with incremental volume changes corresponding to one degree of crankshaft rotation. This was done through 360°, or one full compression and expansion stroke. For each incremental volume change (ΔV) the cylinder conditions were first modeled as a constant volume heat transfer process, followed by a polytropic expansion or compression process for the volume change, as shown in Figure 7.

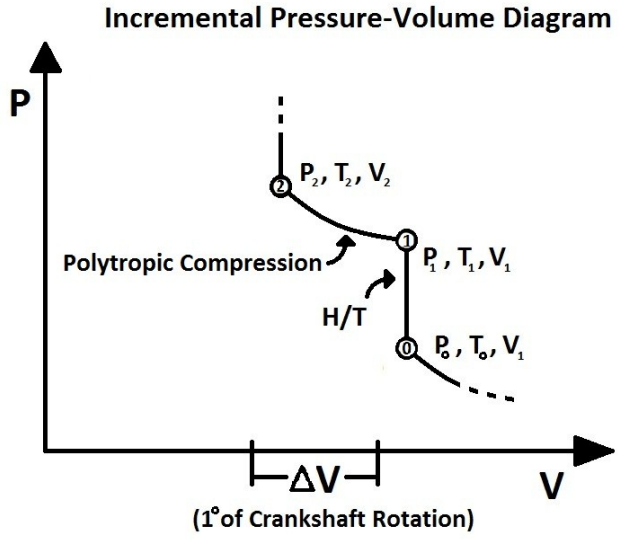

Figure 7. Incremental step in the compression stroke. A single crankshaft angle increment is shown for clarity.

Work energy transfer to or from the gas was calculated using the average pressure across each step and the one preceding it, and multiplying by the incremental volume change.

The pressure in the cylinder was initialized to be a typical atmospheric pressure (14.46 psi), and the temperature 70°F, 530R at the start of the compression cycle, with the pressure remaining constant in the cylinder until the intake valve had substantially closed. Based on engine geometry from an experimental engine, the spark plug was chosen to fire at 30° before TDC, corresponding to a crank angle of 330°.

The heat transfer calculation utilized a simplified form of the Woschni correlation for instantaneous spatial average heat transfer coefficients. Ignoring the second order effects, the Woschni correlation for heat transfer coefficients at each crankshaft increment became the expression shown in Equation 12.

$$h_n = 0.574 * B^{-0.2} * {P_n}^{0.8} * {T_n}^{-0.55} * \left(\frac{2.28\pi}{15} * S * RPM\right)^{0.8} \qquad (12)$$

Using the equation 12 heat transfer coefficient, the heat transfer rate to and from the cylinder walls was calculated assuming an average cylinder wall temperature of 1500 R. The quantity of heat energy transferred to or from the air-fuel mixture was calculated for each step knowing the heat transfer rate and the incremental time unit. The surface area was dependent upon the position of the piston.

$$Area_{s_n} = A_{Piston} + A_{head} + \pi * B * (X_{TDC} - X_\theta) \quad (13)$$

$$\dot{Q}_{H/T_n} = h_{n-1} * Area_{s_n} * (T_{wall} - T_{n-1}) \quad (14)$$

$$Q_{H/T_n} = \dot{Q}_{H/T_n} * \frac{\Delta t}{3600} \quad (15)$$

An additional heat energy term to the air from fuel combustion, (Q_{comb}) was also added. The heat from combustion was estimated based on a stoichiometric octane fuel mixture being provided by the carburetor, and an average fuel burn curve (Figure 8) obtained from *Internal Combustion Engine Fundamentals*, by J.B. Heywood.

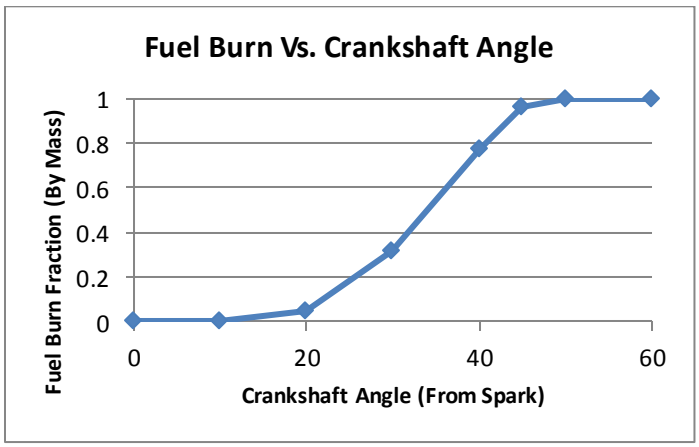

Fig. 8, Mass fraction of fuel burned since ignition, measured in crankshaft degrees. (Octane) [1]

[1] Heywood, J. B. *Internal Combustion Engine Fundamentals.* New York: McGraw-Hill, 1988. Print.

The mass of air in the cylinder was modeled with the ideal gas law, assuming a completely filled cylinder at bottom dead center and using the air pressure and temperature at BDC before the compression stroke. The mass of fuel was then calculated based on the molecular weight of fuel, and a stoichiometric 14.7:1 air-fuel ratio. Using a lower heating value of 19,100 Btu/lbm, and the discrete cumulative distribution of fuel burned by mass in 10^{o} rotation increments taken from Figure 8, a more realistic, non-instantaneous combustion process was modeled. An example of this calculation for θ between 10° and 20° after ignition is shown in Equation 16.

$$Q_{comb_{n_{(10^{\circ}-20^{\circ})}}} = \frac{Burn\ Frac_{\theta_i+20^{\circ}} - Burn\ Fraction_{\theta_i+10^{\circ}}}{10} * M_{fuel} * LHV \qquad (16)$$

With the constant volume heat transfer accounted for in each step, the temperatures and pressures in the cylinder then had to be determined. After the heat energy transferred to or from the cylinder walls, as well as any combustion energy had been added, and the air fuel mixture had been quantified, the internal energy contribution of the total heat transferred was calculated (Equation 17).

$$\Delta u_n = \frac{Q_{comb_n} + Q_{H/T_n}}{M_{air}} \qquad (17)$$

Then, because the heat transfer at each step in the model was treated as the constant volume process of an ideal gas, the internal energy at the start of each step in the cycle could also be computed solely as a function of temperature. With the final temperature

from the previous step, and knowledge of the internal energy function with temperature for air, the internal energy at the start of each step was determined.

Knowing the internal energy of the air/fuel mixture quantified at the beginning of each step, u_{n_0}, and the change in internal energy due to heat transfer and combustion effects, Δu_n from Equation 17, a new internal energy value was expressed by u_{n_1} (Equation 18).

$$u_{n_1} = u_{n_0} + \Delta u_n \tag{18}$$

Temperatures and pressures were found at the end of the constant volume process by solving for the temperature T_1, corresponding to u_{n_1}, and then solving for P_1 using:

$$P_1 = P_0 * \frac{T_1}{T_0} \tag{19}$$

With the pressure, temperature, internal energy, and volume computed at the end of the constant volume process, the model then considered the polytropic expansion or compression process, across the incremental volume change.

The pressure change caused by the piston movement was calculated, considering the air/fuel mixture to be an ideal gas with a polytropic index of $n = 1.3$, slightly less

than the isentropic index, to account for the rapid expansion of the exhaust gasses, causing non-idealities[2] (Equation 20).

$$P_{n_2} = P_{n_1} * \left(\frac{V_{n-1}}{V_n}\right)^{1.3} \tag{20}$$

Boundary work done by the trapped gas was calculated taking the average pressure across the completed step, $P_{avg} = (P_0 + P_1)/2$, and multiplying by the incremental change in volume.

$$W_{net} = P_{avg} * (\Delta V) \tag{21}$$

Finally, using the energy inputs $Q_{H/T}$, Q_{comb} and W_{net} along with the initial internal energy u_{n0}, the value for u_{n2} was calculated using the First Law.

$$u_{n_2} = u_{n_0} + \frac{Q_{H/T} + Q_{comb} - W_{net}}{M_{air}} \tag{22}$$

This final internal energy value, u_{n_2}, was used in calculating T_{n_2}. The values of T_{n_2}, P_{n_2}, and W_{net} then served as inputs to the next incremental volume change step.

Both the circular path model and the epitrochoidal path model were produced similarly, with the only variation being path difference. Once these calculations were completed for each crankshaft angle degree between 0° and 360°, the work done by the

[2] Heywood, J. B. *Internal Combustion Engine Fundamentals.* New York: McGraw-Hill, 1988. Print.

gas on the piston was simply summed, and the resulting net work converted to horsepower production at 3600RPM, completing the basic thermodynamic model for both cycles.

ADDITIONAL CONSIDERATIONS TO IMPROVE MODEL ACCURACY

VALVE TIMING

Valve timing plays a major role in the power output of an internal combustion engine. To limit the error associated with assuming an instantaneous movement, valve movement times were measured on the test engines. The valve movement with respect to crankshaft angle was shown to be equal for both engines, since the valve heads and cam shafts were identical.

Although the intake valve closes gradually, the intake stroke was treated ideally changing from fully open to fully shut at 232 degrees, the crankshaft angle corresponding 0.005 inches of valve lift. This was accomplished by modeling the air inside the cylinder at a constant, atmospheric pressure before the valve closed, and then starting the compression process at the 232 degree location.

The exhaust valve was treated with a slightly more complex process. The valve was modeled as completely sealed until 113 degrees, corresponding to 0.002 inches of valve lift, and gradually opening until a crankshaft angle advanced to 164 degrees. During the valve's gradual opening, the remaining pressure in the cylinder was reduced linearly from the cylinder pressure to atmospheric pressure.

VOLUMETRIC EFFICIENCY

One of the advantages claimed for the epitrochoidal engine is an increased volumetric efficiency. Volumetric efficiency is a measure of the volume of air taken in by a cylinder at a given RPM compared to the maximum capacity of the cylinder at BDC at atmospheric pressure. Volumetric efficiency has a direct scaling effect in output horsepower, by scaling the amount of fuel/air mixture used in the cycle. More complete intake of fuel/air, in turn, means an increase in power produced by the cycle. An analysis of this effect was a critical inclusion in the comparative thermodynamic model.

In order to establish an estimate of the volumetric efficiency differences between the two engines, two methods of analysis were implemented: a volume comparison at valve closure, and numerical time-volume integration of the intake stroke. If the assumption is made that the cylinders are completely filled at bottom dead center (180^{o} crank angle), then any reduction in the volume of air as the piston rises before the intake valve is completely closed represents a loss of combustion reactants through the intake valve (Shaded region in Figure. 2). The difference in the volumetric loss of these combustion reactants was characterized as a percentage of total volume. Using this volumetric comparison method, the epitrochoidal cycle was found to experience a volumetric loss at the start of its compression cycle that was approximately 16.7% less than the standard cycle's volumetric losses. This means that the epitrochoidal dwell around BDC results in 16.7% more air remaining in the cylinder.

To verify the volumetric comparison method, discrete time-volume integration for the intake stroke was also calculated. The volume of the cylinder during the intake stroke was assumed to be related to the pressure difference between the cylinder and the atmosphere, and the more time spent at a specific cylinder volume, the more completely that fixed volume fills with combustion reactants. A piston which dwells longer near the bottom of the stroke would therefore fill more completely for a given air intake system. The time-volume integrations took the volume of the epitrochoidal cylinder and the volume of the stock cylinder independently and numerically integrated those volumes over the entire intake strokes. Once this was complete, the relative improvement of the epitrochoidal path over the stock piston path was determined. The results of this calculation were that the epitrochoidal cylinder dwelled beneath the standard cycle by about 17%, very similar to the previous method.

FRICTIONAL LOSSES

The gear system required to produce an epitrochoidal path imposes more frictional loss than the standard crank. To account for these losses, experiments were run to measure friction losses. Using an electric motor to drive the crankshaft of each engine, separately (with the spark plug removed), the power supplied to the electric motor was measured. Knowing the efficiency of the drive motor allowed the total power supplied to the crankshaft of each test engine to be determined. The spark plug was removed from the engine under test in an attempt to isolate friction losses from power losses due to compression. Because of the drive motor size limitation, the frictional power losses curves could be determined only for speeds less than 1000 RPM. Therefore, the power loss curves were extrapolated to 3600 RPM, assuming the frictional losses increased linearly with rotational speed and were zero at 0 RPM (Figure 9). At 3600 RPM, these losses were measured to be 0.51Hp for the standard and 1.33Hp for the epitrochoidal cycle.

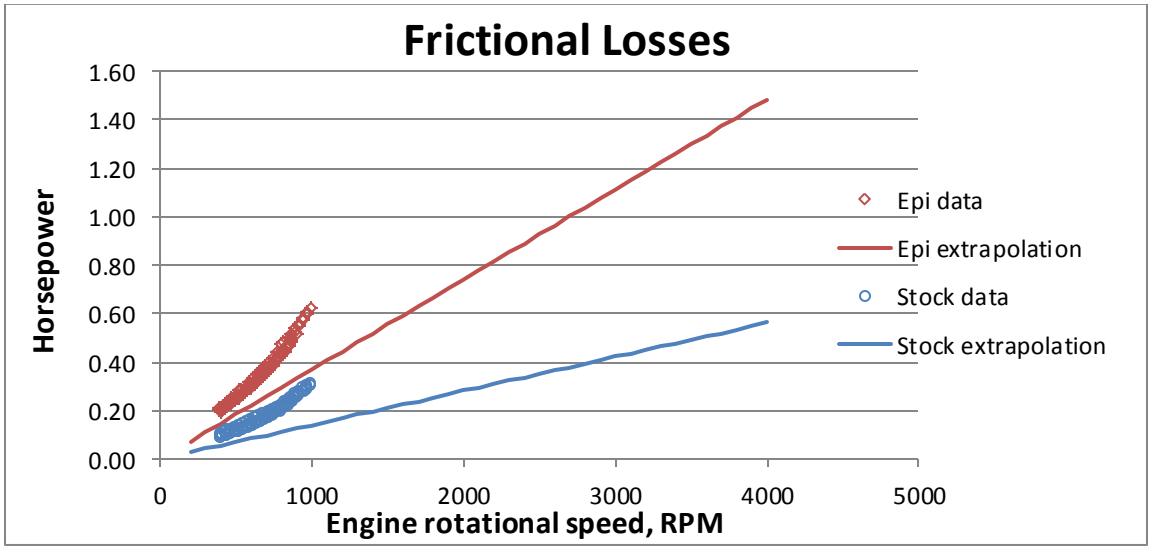

Figure 9. Frictional Loss Curves

RESULTS AND DISCUSSION

An intermediate result of the theoretical models were a pressure-volume curve for both engine cycles (Figure 10), as well as a numerical integration of these two curves to obtain the gross power output of each engine.

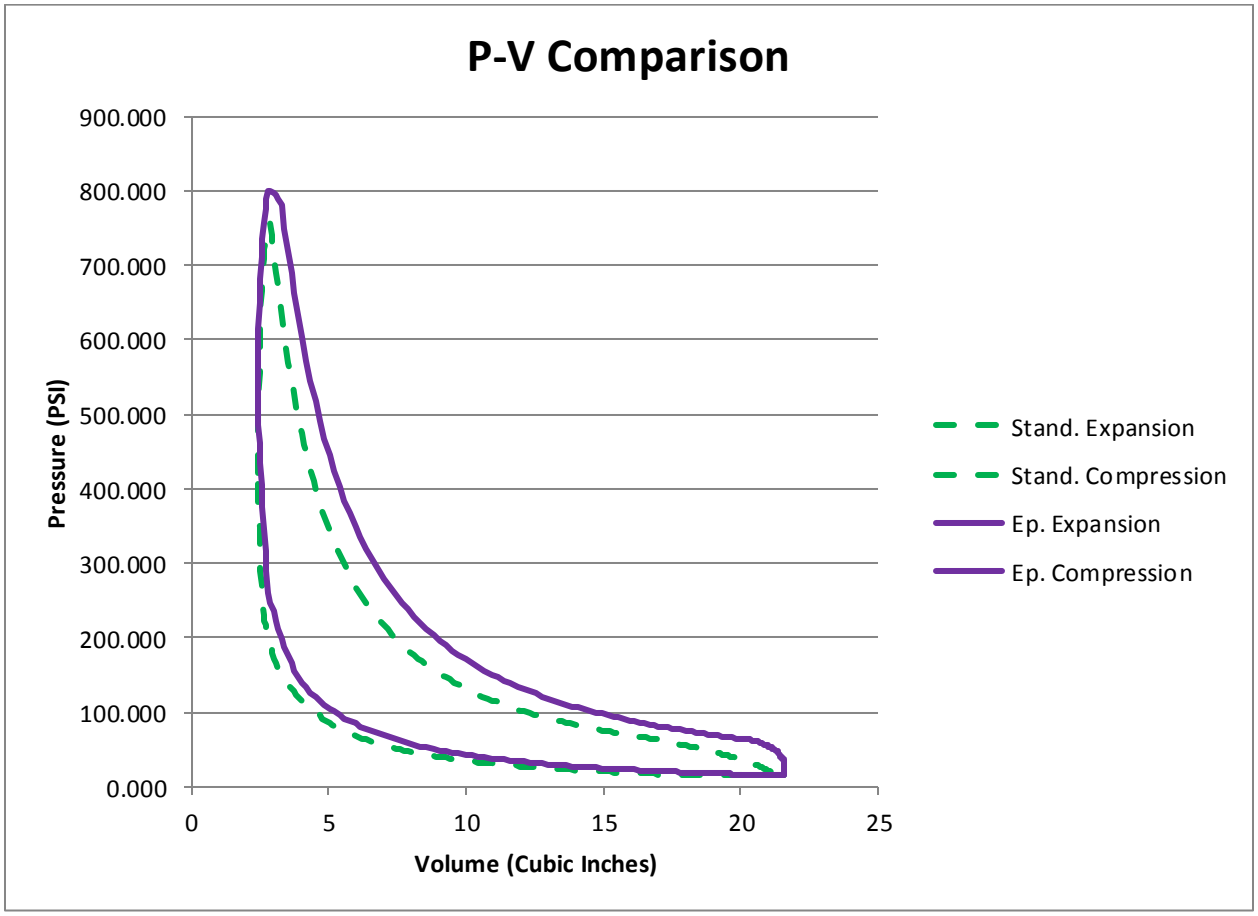

Figure. 10, Final Pressure-Volume Curve Comparison

While these two curves do not yet account for differing frictional losses, they still show the general trends taking place in each stroke and highlight the differences between the epitrochoidal and standard cycles.

As shown in the completed pressure-volume diagram in Figure 10, several differences were evident which affect the predicted gross power output. At the start of the combustion cycle, the pressure was increased in the cylinder in preparation for combustion. This pressure was increased for the epitrochoidal engine during the compression stroke because of the greater volume of trapped fuel/air mixture in the cylinder. This effect taken alone detracted from the power output of the epitrochoidal cycle because more work was spent compressing incoming air, but allowed for greater mass flow through the engine. Also this increase in fuel/air mixture led to a predicted increase in peak combustion pressure over the standard cycle.

Combustion at the end of the compression stroke and during the start of the expansion stroke was also affected by the change in cycle path. The pressure peak was not only higher in the epitrochoidial path, but it also occurred slightly later in the expansion stroke, peaking at 2.74 cubic inches of piston volume compared to 2.62 cubic inches for the standard cycle. This difference occurred because the piston's dwell time at top dead center was shorter in the epitrochoidal cycle than in the standard cycle, which limited the percentage of combustion taking place at or near the minimum volume; this would normally decrease the total pressure developed by the cycle during the exhaust stroke, but because of the increase in mass flow, the total pressure developed in the experimental cycle was still higher than the standard cycle. In this model the predicted temperatures during the combustion phase of each cycle approached 3600ºF. These high predicted temperatures were somewhat unrealistic because the model ignored the chemical recombination energy, and other losses involved with real combustion processes, and instead assumed ideal gas (air) behavior through the cycle.

This assumption was made to simplify the comparative model, but the energy losses associated with real combustion process would serve to lower the maximum temperature in practice. The pressure was taken to be accurate because the pressure of the gas is heavily dependent on the number of molecules before and after the reaction, and not as heavily dependent on the stored thermal energy of each molecule.

The increase in maximum combustion pressure for the epitrochoidal cycle also caused a higher pressure for the entire expansion stroke. Because of the higher initial pressure, the pressure on the piston remained elevated above the standard cycle pressure throughout the power stroke. This additional epitrochoidal cycle pressure could be seen through comparison of the top portion of each curve in Figure 10.

Finally, the effects of the exhaust valve opening characteristics could be seen towards the end of the expansion stroke. Because of the valve characteristics, pressure in the cylinder began to drop towards atmospheric pressure linearly as the exhaust valve opened. This effect was present in both the standard and epitrochoidal cycles, but because the piston fell faster on the power stroke in the epitrochoidal cycle the piston was able to fall farther while still under pressure than with the standard cycle. This meant that more useful energy could be extracted from the pressurized combustion products before they were vented to the atmosphere.

When the combination of all these effects, positive and negative, was represented in the model, and then the area of the resulting Pressure-Volume curve was numerically integrated by crankshaft degree to obtain a work produced by the cycle, the work produced by the epitrochoidal path in one cycle was larger than the work produced by the standard cycle. The raw, gross horsepower output was 9.90 Hp at 3600 RPM for the

standard cycle power output, compared to an epitrochoidal cycle power output of 12.48 Hp at 3600 RPM. This means the predicted comparison models showed a gross power increase of approximately 26% for the epitrochoidal engine.

The frictional losses of each engine, 0.51 Hp and 1.33 Hp for the standard and epitrochoidal cycles, respectively, were then subtracted from the predicted raw horsepower to obtain a predicted net horsepower to the load. Though the frictional losses for the epitrochoidal engine cycle were over twice that of the standard engine, there was still a predicted net horsepower increase of 18.7% for the epitrochoidal engine.

CONCLUSION AND COMMENTS

One of the potential improvements of the epitrochoidal piston path over the standard circular path is the increase in trapped (or effective) compression ratio, or the ratio of the volume trapped when the intake valve closes on the intake stroke to the volume of the cylinder at top dead center. This increase in effective compression ratio led to a power loss on the compression stroke compared to a standard circular path, but a significant increase in cylinder pressure after combustion, resulting in a net power gain for the cycle. In total, holding everything constant except the crankpin path, a power increase of 18.7% was predicted.

One suggestion for future study that could further understanding of non-circular cycle engines is adding mass-flow sensors to the fuel and air intake on an experimental epitrochoidal engine, allowing an accurate volumetric flow rate to be determined for a more complete model. Another suggestion is to add internal pressure and temperature sensors inside the cylinder, to accurately measure flame temperature of each engine, allowing real efficiencies and energy balance equations to be discussed in a semi-empirical model. Lastly, lifecycle research on the gearing involved in the creation of the epitrochoidal path would enable more informed decisions on the viability of non-circular paths for future engine production designs.

ABSTRACT

A thermodynamic performance model has been developed for a new four-stroke engine design in which the crank shaft path is non-circular (epitrochoidal). First, a mathematical description of the piston path was defined, identifying the piston path and cylinder volume as functions of engine geometry and crankshaft angle. The modeling approach was also used to develop a standard circular path performance as a comparison. The result was two discrete models, varying only in piston path. Fundamental effects included in both models were valve and spark timing, heat transfer to and from the engine block, volumetric efficiency, and spark ignition combustion timing. In addition to these considerations, frictional losses were measured experimentally on a standard spark ignition engine and an also an epitrochoidal prototype engine using the same cylinder head. The frictional losses were then included in the model. Predicted performance results were used in support of experimental testing of the standard and prototype epitrochoidal engines. These comparative thermodynamic models have been used to explain the changes in performance caused by an epitrochoidal crankshaft design. This report will include the development of the mathematical model for piston movement, comparisons of epitrochoidal and standard path cycle pressures and temperatures, as well as predicted and measured power outputs for both engines.